CELL BIOLOGY

Regulated N-glycosylation controls chaperone function and receptor trafficking

Mengxiao Ma[1], Ramin Dubey[1], Annie Jen[2], Ganesh V. Pusapati[1], Bharti Singal[3], Evgenia Shishkova[4,5], Katherine A. Overmyer[2,5], Valérie Cormier-Daire[6], Juliette Fedry[7], L. Aravind[8], Joshua J. Coon[2,4,5,9], Rajat Rohatgi[1]*

One-fifth of human proteins are N-glycosylated in the endoplasmic reticulum (ER) by two oligosaccharyltransferases, OST-A and OST-B. Contrary to the prevailing view of N-glycosylation as a housekeeping function, we identified an ER pathway that modulates the activity of OST-A. Genetic analyses linked OST-A to HSP90B1, an ER chaperone for membrane receptors, and CCDC134, an ER luminal protein. During its translocation into the ER, an N-terminal peptide in HSP90B1 templates the assembly of a translocon complex containing CCDC134 and OST-A that protects HSP90B1 during folding, preventing its hyperglycosylation and degradation. Disruption of this pathway impairs WNT and IGF1R signaling and causes the bone developmental disorder osteogenesis imperfecta. Thus, N-glycosylation can be regulated by specificity factors in the ER to control cell surface receptor signaling and tissue development.

N-glycosylation influences a myriad of processes, including development, cell-cell recognition in the immune system, inflammatory responses, and the metastatic spread of cancer cells (*1*, *2*). The dominant view in cell biology has been that N-glycosylation is a constitutive process initiated by two multisubunit oligosaccharyltransferase complexes, OST-A and OST-B, that contain the distinct catalytic subunits STT3A and STT3B, respectively (*3*). OST-A contains distinct subunits (OSTC and KRTCAP2) that anchor it to the SEC61 protein channel (*4*), and it functions cotranslationally to transfer a preassembled glycan from a lipid donor to asparagine residues found in the context of N-X-S/T/C sequons (where X can be any residue other than proline). The catalytic site in STT3A is positioned at the luminal surface of the endoplasmic reticulum (ER) membrane to scan the nascent chain for sequons as it emerges from SEC61 (*5*–*8*). OST-B functions co- or posttranslationally on sequons missed or poorly recognized by OST-A (*3*). A notable unanswered question is whether the activity of the OST-A and OST-B complexes, which sit at the apex of the N-glycosylation pathway, can be controlled by other factors to switch the glycan occupancy of specific sequons on or off.

[1]Departments of Biochemistry and Medicine, Stanford University School of Medicine, Stanford, CA 94305, USA. [2]Department of Biomolecular Chemistry, University of Wisconsin, Madison, WI 53506, USA. [3]Stanford SLAC CryoEM Initiative, Stanford, CA 94305, USA. [4]National Center for Quantitative Biology of Complex Systems, Madison, WI 53706, USA. [5]Morgridge Institute for Research, Madison, WI 53515, USA. [6]Université Paris Cité, Génétique clinique, INSERM UMR 1163, Institut Imagine, Hôpital Necker-Enfants Malades (AP-HP), Paris, France. [7]MRC Laboratory of Molecular Biology, Cambridge CB2 0QH, UK. [8]Computational Biology Branch, Division of Intramural Research, National Library of Medicine, National Institutes of Health, MD 20894, USA. [9]Department of Chemistry, University of Wisconsin, Madison, WI 53506, USA.
*Corresponding author. Email: rrohatgi@stanford.edu

Genetic screens identify ER-localized regulators of WNT signaling

Using a fluorescence-based transcriptional reporter, we conducted a genome-wide, loss-of-function CRISPR-Cas9 screen in a human cell line (RKO) to identify genes required to activate WNT/β-catenin signaling in response to WNT3A (fig. S1A and data S1) (*9*). The screen identified known WNT signaling components (fig. S1, B and C): β-catenin, LRP6 (a coreceptor for WNT ligands), and two ER chaperones, MESD and HSP90B1, that facilitate LRP5 and LRP6 folding in the ER (*10*, *11*). Our screens also identified three genes not linked to WNT signaling: *CCDC134*, *STT3A*, and *OSTC* (fig. S1, B to D). STT3A and OSTC are two subunits of the OST-A (but not the OST-B) complex. CCDC134 is a poorly studied protein required for mouse embryonic development (*12*). Based on correlated patterns of essentiality across >1000 cell lines in the Cancer Dependency Map (DepMap), *CCDC134*, *STT3A*, and *OSTC* clustered with each other and the LRP6 chaperone HSP90B1 (Fig. 1A) (*13*, *14*).

Whereas STT3A, OSTC, and HSP90B1 are established ER proteins, CCDC134 is annotated as both a secreted cytokine and a nuclear protein in Uniprot (*15*, *16*). However, CCDC134 contains signal sequences for both ER targeting and retention (fig. S1E). CCDC134 is indeed a protein resident in the ER; mutation of its C-terminal "QSEL" ER-retention sequence to "QSSA" abrogated its ER retention and enabled its secretion into the media (fig. S1, F and G).

Regulation of the ER chaperone HSP90B1 by hyperglycosylation

Disruption of *STT3A* (but not of *STT3B*) paradoxically results in the hyperglycosylation and destabilization of HSP90B1 (*17*). We reproduced this observation and, to our surprise, found that disruption of *CCDC134* and *OSTC* had a similar effect, supporting DepMap's prediction of a shared function amongst these proteins (Fig. 1, B and C). Additionally, disruption of *STT3A*, *CCDC134*, or *OSTC* reduced the abundance of the WNT coreceptor LRP6 at the cell surface (Fig. 1B), explaining why loss of these proteins impaired responses to WNT ligands in our screen (fig. S1, C and D).

The function of HSP90B1 hyperglycosylation and how it is regulated is unclear (*17*–*21*). HSP90B1 has six conserved glycosylation sites (Fig. 1D and fig. S2A). One of these sequons (N217) is constitutively modified with an N-glycan (hereafter called the "constitutive sequon"), whereas five (N62, N107, N445, N481, and N502) are only used under specific conditions (hereafter called "facultative sequons") (*17*, *18*, *20*). HSP90B1 is hyperglycosylated when its abundance increases, either when it is overexpressed or when its transcription increases in response to ER stress (*18*).

Facultative sequons are located in regions of HSP90B1 that would be predicted to impair protein function or folding (*18*) (fig. S2A). This arrangement is unusual: in most secretory pathway proteins, sequons have been depleted during evolution from buried regions of proteins (*22*). Hyperglycosylated HSP90B1 cannot fold into a functional protein, causing it to be flagged and degraded by ER-associated protein degradation (ERAD) (fig. S2B).

Global N-glycoproteomics revealed both highly specific and concordant effects of STT3A and CCDC134 on the N-glycosylation of HSP90B1 (*23*). Out of ~4000 N-glycopeptides identified across the proteome, those derived from HSP90B1 showed the greatest increase in abundance in *CCDC134*$^{-/-}$ and *STT3A*$^{-/-}$ cells compared with wild-type cells (Fig. 1, E and F, and data S2), even though the overall abundance of HSP90B1 was reduced in both mutant cell lines (Fig. 1C). N-glycopeptides enriched in the mutant cell lines encompassed one of the five facultative sequons of HSP90B1 (Fig. 1G). By contrast, the abundance of N-glycopeptides containing the single constitutive sequon (N217) did not change in *CCDC134*$^{-/-}$ and *STT3A*$^{-/-}$ cells compared with that in wild-type cells (Fig. 1G)

Regulation of WNT reception at the cell surface by CCDC134 in the ER

Because the function of CCDC134 was unknown, we investigated its role in WNT signaling in more detail. Disruption of *CCDC134* in multiple mouse and human cell lines resulted in HSP90B1 hyperglycosylation and destabilization (Fig. 1H and fig. S3, A to F). Stable reexpression of CCDC134 at near-endogenous levels by using a doxycycline-inducible system (fig. S3G) suppressed both HSP90B1 hyperglycosylation and restored its abundance (Fig. 1I). Additionally, the coexpression of CCDC134 suppressed HSP90B1 hyperglycosylation caused by its overexpression (fig. S3H) and had a dose-dependent protective effect on HSP90B1 in the face of ER stress (fig. S3I).

Cell surface LRP5 and LRP6 abundances were markedly reduced in *CCDC134*$^{-/-}$ cells (Fig. 1J). Electrophoretic mobility and glycosylation analyses demonstrated that LRP6 was trapped in the ER (Fig. 1K) (*24*). Consequently, *CCDC134*$^{-/-}$ cells were less responsive to WNT ligands than wild-type cells, which was measured by WNT reporter activity (fig. S1C) or β-catenin protein accumulation (Fig. 1L). WNT signaling sensitivity could be restored by reexpressing wild-type CCDC134 but not mutants that lacked either the signal sequence for its ER targeting or the QSEL sequence for its ER retention (fig. S3, J and K). Thus, CCDC134 regulates WNT signaling in the ER by controlling the trafficking of LRP5 and LRP6, obligate coreceptors for WNT ligands, to the cell surface.

To establish organism-level functional and disease relevance, we used primary fibroblasts from two human patients carrying loss-of-function mutations in CCDC134 (*25*). CCDC134 mutations have been identified as a rare cause of the bone developmental disorder osteogenesis imperfecta (OI) in five patients from three families (*25*–*27*). These patients suffer from a severe, deforming subtype of OI (Type III) that is also seen in patients carrying mutations in other WNT pathway genes, such as *MESDC2* and *WNT1* (*28*). Primary fibroblasts from *CCDC134*$^{-/-}$ patients demonstrated HSP90B1 hyperglycosylation, reduced cell surface LRP6 abundance, and impaired WNT signaling. All defects were reversed upon the reexpression of CCDC134 (fig. S4).

Genetic interactions organize CCDC134, OST-A, and HSP90B1 into a pathway

To test whether hyperglycosylation of HSP90B1 was the root cause of reduced cell surface LRP6 and WNT sensitivity in *CCDC134*$^{-/-}$ cells, we disrupted all five facultative sequons in HSP90B1 (hereafter called the HSP90B1^{5N} mutant) (Fig. 1D). As a control, we separately disrupted the single constitutive sequon (N217, mutated in HSP90B1^{1N}). Both HSP90B1^{5N} and HSP90B1^{1N} were functional proteins because they were expressed at levels comparable to wild-type HSP90B1 (fig. S5A) and rescued cell-surface LRP6 and WNT signaling in *HSP90B1*$^{-/-}$ cells (Fig. 2, A and B). However, only HSP90B1^{5N} (but not wild-type HSP90B1 or HSP90B1^{1N}) rescued *HSP90B1*$^{-/-}$;*CCDC134*$^{-/-}$ double-null cells, formally showing that *HSP90B1* is epistatic to *CCDC134* in the WNT pathway.

Analogous to the loss of either CCDC134 or HSP90B1, disruption of *STT3A* (but not *STT3B*) also markedly reduced cell surface LRP6 and the strength of WNT signaling (Fig. 2, C and D). Notably, HSP90B1^{5N} expression was sufficient to completely rescue WNT signaling in *STT3A*$^{-/-}$ cells (Fig. 2, C and D), despite the fact that the N-glycosylation of hundreds of proteins is altered when OST-A function is lost (*17*). The depletion of functional HSP90B1 in *STT3A*$^{-/-}$

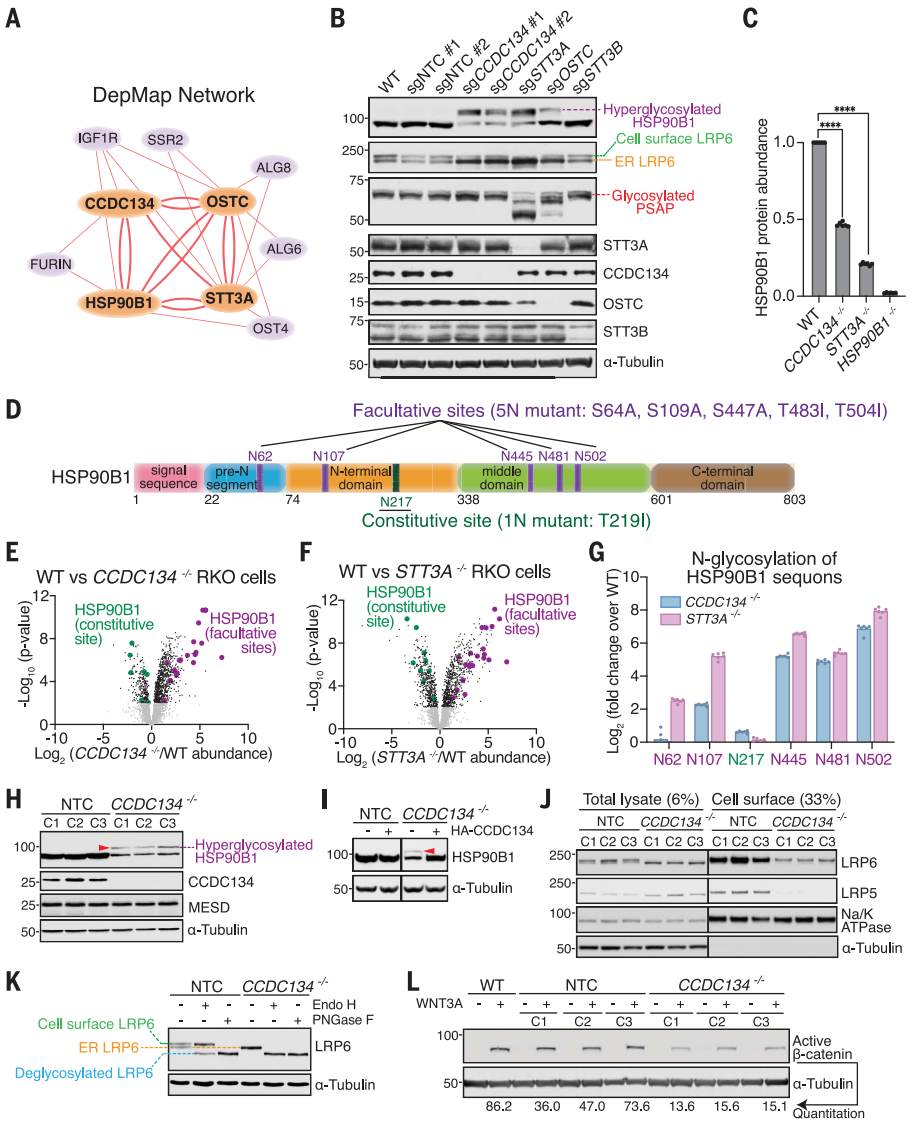

Fig. 1. Regulation of HSP90B1 N-glycosylation and WNT signaling by an ER protein network. (**A**) DepMap cluster showing bidirectional interactions between *CCDC134*, *STT3A*, *HSP90B1*, and OSTC. (**B**) Abundances and glycosylation status of HSP90B1, its client LRP6, and PSAP (an exclusive OST-A substrate) in cells expressing single guide RNAs (sgRNAs) against the indicated genes. NTC, nontargeting control. (**C**) HSP90B1 protein abundance measured by mass spectrometry, normalized to wild-type (WT) cells. Bars represent the mean (N = 6). ****P < 0.0001 [one-way analysis of variance (ANOVA) with Dunnett's test]. (**D**) Domain architecture of HSP90B1 showing the one constitutive (green) and five facultative (purple) N-glycosylation sites along with the mutations used to disrupt them (1N and 5N mutants). See fig. S2A for a structural view. (**E** and **F**) Abundances of glycosylated peptides in *CCDC134*$^{-/-}$ (E) and *STT3A*$^{-/-}$ (F) cells measured using global, unbiased N-glycoproteomics. Each data point represents the fold change in abundance of a distinct glycopeptide in mutant compared with wild-type cells. The full dataset is in data S2. (**G**) Enrichment of glycopeptides (normalized to total HSP90B1 protein abundance) that include each of the facultative and constitutive sequons of HSP90B1 in *CCDC134*$^{-/-}$ or *STT3A*$^{-/-}$ cells. Bars show the mean (N = 6). (**H** and **I**) Abundance and glycosylation status of HSP90B1 in lysates from three (C1 to C3) independent control (NTC) and *CCDC134*$^{-/-}$ clonal cell lines (H) or after the stable expression of human influenza hemagglutinin (HA)–tagged CCDC134 in *CCDC134*$^{-/-}$ cells (I). The hyperglycosylated form of HSP90B1 is indicated with a red arrowhead. (**J**) LRP6 and LRP5 abundances in total lysate or at the plasma membrane from three independently derived (C1 to C3) control (NTC) or *CCDC134*$^{-/-}$ clonal cell lines. (**K**) Glycosidase sensitivity in conjunction with mobility on SDS–polyacrylamide gels was used to measure the ER or cell-surface pools of LRP6 in control or *CCDC134*$^{-/-}$ cells. Glycans on cell-surface proteins are Endoglycosidase H (Endo H) resistant and Peptide:N-glycosidase F (PNGase F) sensitive; those on ER proteins are sensitive to both enzymes. (**L**) Active (nonphosphorylated) β-catenin abundance (a metric of WNT signaling strength) was measured (±WNT3A) by using immunoblots in wild-type cells or three independent (C1 to C3) clonal cell lines expressing a control (NTC) sgRNA or an sgRNA targeting *CCDC134*. Single-letter abbreviations for the amino acid residues referenced throughout this paper are as follows: S, Ser; R, Arg; T, Thr; N, Asn; P, Pro; A, Ala; L, Leu; I, Ile.

and *CCDC134*$^{-/-}$ cells would be predicted to impair the cell surface trafficking and signaling capacity of other signaling receptors known to be its clients (*29*–*31*). CCDC134 and STT3A are required for the cell surface expression of TLR4, a HSP90B1 client and receptor for bacterial endotoxins that activates inflammatory signaling through the NF-κB pathway (*32*). DepMap analysis also predicted a functional link between IGF1R (another HSP90B1 client) and the CCDC134–OST-A cluster (Fig. 1A). Analogous to LRP6, cell surface expression of IGF1R was disrupted by the loss of either CCDC134 or STT3A but could be rescued by expression of HSP90B1^{5N} (fig.S5, B to D) (*33*).

There was a notable difference in HSP90B1 N-glycosylation in *STT3A*$^{-/-}$ cells compared with that in *CCDC134*$^{-/-}$ cells. The entire pool of HSP90B1 was hyperglycosylated in the former, whereas only a fraction was hyperglycosylated in the latter (Fig. 2E). Even a massive increase in CCDC134 abundance was unable to suppress HSP90B1 hyperglycosylation in *STT3A*$^{-/-}$ cells (Fig. 2E). These data suggest that OST-B (the only OST complex left in *STT3A*$^{-/-}$ cells) fully N-glycosylates HSP90B1 by default at all sequons and cannot be regulated by CCDC134. In *STT3B*$^{-/-}$ cells, loss of CCDC134 leads to HSP90B1 hyperglycosylation, showing that CCDC134 regulates OST-A (Fig. 2E).

These epistasis relationships allow the assembly of *CCDC134*, *HSP90B1*, and *STT3A* into a provisional genetic pathway (Fig. 2F) that can communicate the integrity of N-glycosylation to reception of WNT signals at the cell surface. This pathway model served as a framework for our subsequent biochemical studies.

An N-terminal unstructured peptide in HSP90B1 regulates its own N-glycosylation

We next turned to investigate the question of whether sequence elements within HSP90B1 regulate its own N-glycosylation. To simplify glycosylation analysis by gel shift analysis, we used a HSP90B1 variant carrying only three facultative sequons located in its middle (M) domain (Fig. 3A). The M domain alone was efficiently hyperglycosylated but completely resistant to CCDC134 coexpression (Fig. 3B), showing that sequences distant from the sequons themselves were required. The C-terminal domain (CTD) was dispensable, thereby implicating the N-terminal domain (NTD) and the pre-N segment (fig. S6, A and B).

Deletion analysis revealed that amino acids 1 to 93 (1-93) of HSP90B1, which includes the ER signal sequence and all of the pre-N segment, could affect the N-glycosylation of distant sequons in the M domain (fig. S6C). Deletions that extended into this 1-93 segment enhanced M domain hyperglycosylation. A minimal model substrate, in which the unstructured N-terminal 93 amino acids of HSP90B1 were fused to its M domain carrying three facultative sequons, was used for many of our subsequent experiments (hereafter called 1-93M) (Fig. 3A). The hyperglycosylation of 1-93M was efficiently suppressed by CCDC134, and its shorter length enabled efficient translation and glycosylation analysis by gel electrophoresis (Fig. 3B).

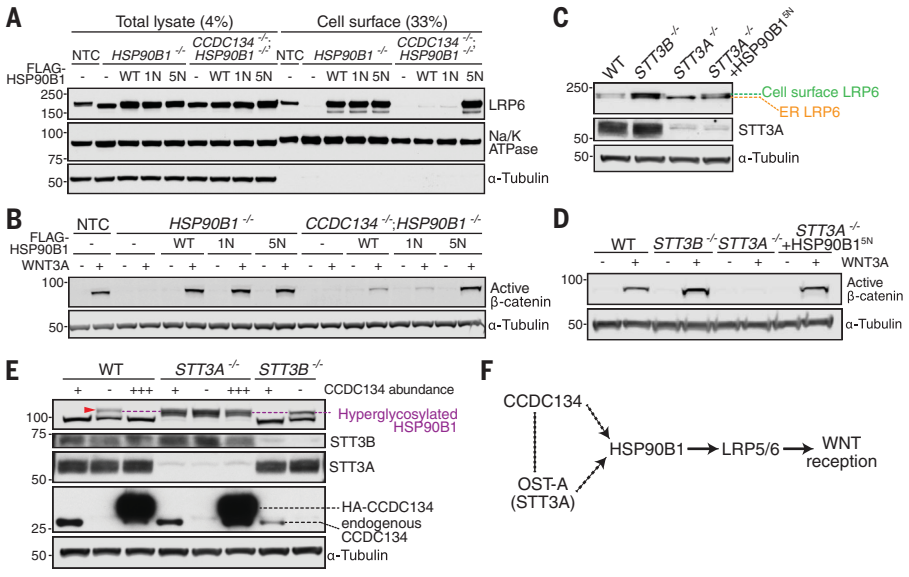

Fig. 2. Hyperglycosylation of HSP90B1 regulates WNT signaling strength. (**A** to **D**) Abundances of cell-surface LRP6 [(A) and (C)] or active β-catenin [(B) and (D)] in clonally derived cell lines of the indicated genotypes stably expressing wild-type FLAG-HSP90B1 or variants carrying mutations in the one constitutive (1N) or all five facultative (5N) sites (Fig. 1D and fig. S2A). HSP90B1 variants were expressed at comparable levels (fig. S5A). Na/K ATPase, sodium and potassium transporting adenosine triphosphatase. (**E**) N-glycosylation status of HSP90B1 in *STT3A*$^{-/-}$ and *STT3B*$^{-/-}$ cells expressing different levels of CCDC134: no CCDC134 was represented by a minus sign (−); endogenous CCDC134, a plus sign (+); and stably overexpressed 3×HA-CCDC134, three plus signs (+++). (**F**) A provisional pathway diagram constructed based on genetic interactions (dotted lines) uncovered in our work, and physical interactions (solid lines) described in the literature.

Alanine scanning mutagenesis of the pre-N segment identified an 18–amino acid stretch following the signal sequence that was important for the suppression of 1-93M hyperglycosylation (fig. S6D). This critical region contains a potential pseudosubstrate sequon [serine-arginine-threonine (SRT) instead of asparagine-arginine-threonine (NRT)] that might bind and inhibit the catalytic activity of STT3A (Fig. 3C). This SRT sequence followed many of the rules of classical sequons. Alteration of the middle R to a proline (P) abolished its ability to inhibit hyperglycosylation. At the third T position, a single conservative change to alanine (hereafter, "T44A") resulted in complete N-glycosylation of 1-93M (Fig. 3C) or of full-length HSP90B1, both at native facultative sequons and at ectopically introduced artificial sequons (fig. S6E). The HSP90B1-T44A mutants were also resistant to CCDC134 regulation, reminiscent of HSP90B1 in *STT3A*$^{-/-}$ cells (Fig. 2E). Notably, these experiments were conducted in *STT3B*$^{-/-}$ cells, showing that the T44A mutation abolishes regulation of HSP90B1 N-glycosylation by both OST-A and CCDC134.

As a final test of the model that the N-terminal 1-93 segment of HSP90B1 functions as a pseudosubstrate inhibitor of the OST-A complex, we transplanted this sequence to prosaposin (PSAP), a protein that carries five sequons glycosylated exclusively by OST-A (Fig. 3D) (*3*, *34*). The 1-93 segment reduced the efficiency of PSAP N-glycosylation (Fig. 3E), just as it reduced the efficiency of M domain N-glycosylation (Fig. 3B). It conferred sensitivity to CCDC134 in a manner that was dependent on the integrity of the SRT pseudosubstrate site (Fig. 3E). Thus, the N-terminal ~93 amino acids of HSP90B1, predicted to be largely unstructured, has two autonomous, transferable properties: It impairs the N-glycosylation of sequons that follow it in the same polypeptide and confers sensitivity to CCDC134 (which further suppresses N-glycosylation).

The observation that a peptide segment can regulate the N-glycosylation of distant sequons that follow it suggested a substrate-directed autoinhibitory model: The N-terminal 1-93 sequence, which emerges from SEC61 into the ER lumen before the M domain, inhibits the ability of OST-A to N-glycosylate any following sequons in the same polypeptide. Cotranslational regulation is an implicit feature of this model and was supported by several observations. Firstly, regulation of HSP90B1 N-glycosylation depended on OST-A (the major cotranslational oligosaccharyltransferase) but not OST-B (which functions posttranslationally): HSP90B1 is fully

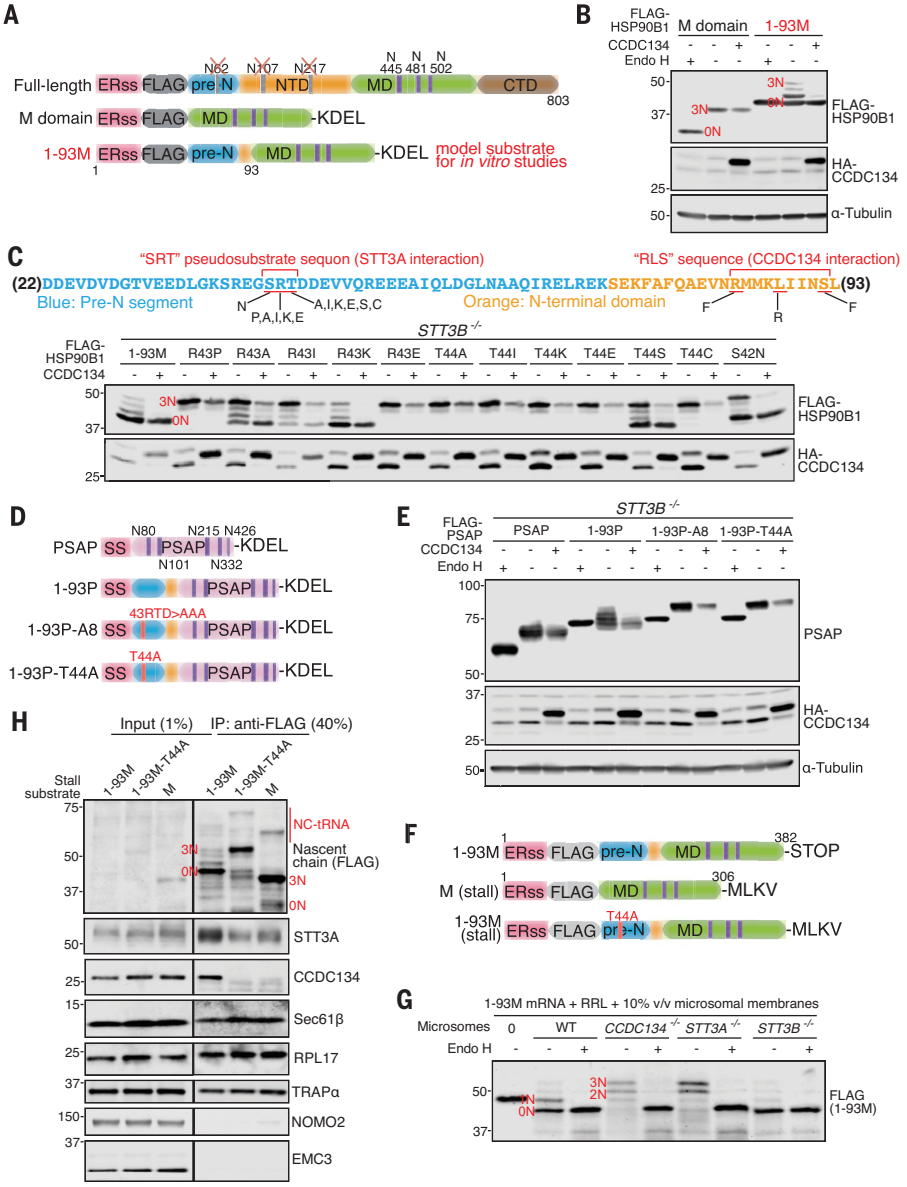

Fig. 3. The pre-N segment of HSP90B1 inhibits its own N-glycosylation by recruiting CCDC134 to an OST-A containing secretory translocon. (**A**) Variants of HSP90B1 used for cell-based and in vitro assays. Key features include: ERss, ER signal sequence; FLAG, 3×FLAG tag; pre-N, unstructured segment; MD, Middle domain. N-glycosylation sites in the pre-N and NTD were eliminated to allow easy assessment of the glycan modification of the three sequons in the M domain by gel shifts [see (B) and text]. KDEL, Lys-Asp-Glu-Leu ER retention signal. (**B**) Glycosylation status of HSP90B1 variants shown in (A) was assessed after transient coexpression in HEK293T cells with wild-type CCDC134 (+) or a nonfunctional variant (−) lacking its ER signal sequence (fig. S3J). Predicted N-glycoforms (carrying zero, one, two, or three glycans) are labeled 0N to 3N in red lettering. (**C**) Glycosylation status of the 1-93M variant [see (A)] of HSP90B1 carrying the indicated mutations in the "SRT" pseudosubstrate motif found in the pre-N segment. See fig. S6, C and D, for deletion and alanine scanning mutagenesis of the pre-N segment. (**D** and **E**) Glycosylation status (E) of chimeric proteins (D) constructed by fusing variants of the 1-93 segment of HSP90B1 to the obligate OST-A substrate PSAP, which contains five N-glycosylation sites shown in (D). T44A changes "SRT" to "SRA," and A8 changes "RTD" to "AAA" [see (C) and fig. S6D]. (**F**) Constructs used for in vitro translation experiments. Translation stall constructs lack a STOP codon. (**G**) Glycosylation status of 1-93M [see (F)] translated in rabbit reticulocyte lysate (RRL) in the presence of rough microsomal membranes generated from wild-type or *CCDC134*$^{-/-}$, *STT3A*$^{-/-}$, or *STT3B*$^{-/-}$ HEK293T cells. Compare to (B). (**H**) Association of endogenous CCDC134 with stalled 1-93M, M the domain alone, or a 1-93M variant carrying a T44A mutation in the "SRT" pseudosubstrate site [see (C) and (F)]. The stalled nascent chain, immunoprecipitated (IP) using anti-FLAG beads, associates with the ribosome (RPL17) and components of the secretory translocon (STT3A, SEC61 channel, TRAP complex) but not with components of the multipass translocon (NOMO2) or the ER-Membrane Protein Complex (EMC3) (*36*, *43*). NC-tRNA, nascent chain–tRNA conjugates.

hyperglycosylated (and resistant to CCDC134) in *STT3A*$^{-/-}$ cells (Fig. 2E). Secondly, depletion of OSTC, which anchors the OST-A complex to the SEC61 channel but is not required for its integrity or catalytic activity (*4*), resulted in HSP90B1 hyperglycosylation (Fig. 1B). Thirdly, expansion of the DepMap network around the CCDC134-STT3A cluster revealed a signature of the ER translocon, including multiple subunits of the TRAP complex (fig. S7A). Lastly, pulse-chase analysis was consistent with cotranslational hyperglycosylation of HSP90B1 in *CCDC134*$^{-/-}$ cells (fig. S7, B and C).

These observations led us to consider the model that the hyperglycosylation of HSP90B1 is regulated by a complex between its own N terminus, CCDC134, and OST-A that assembles during its translation and translocation into the ER. We identified point mutations in both STT3A and the HSP90B1 pre-N segment that blocked CCDC134 activity without disrupting the other functions of these proteins. Mutations in two luminal loops of STT3A (fig. S7, D to F) or in an arginine-leucine-serine (RLS) motif ~40 amino acids distal to the SRT pseudosubstrate (Fig. 3C and fig. S7, G and H) abolished the ability of CCDC134 to suppress HSP90B1 hyperglycosylation. This separation-of-function genetic analysis suggests that HSP90B1 hyperglycosylation involves two ordered (but mutationally separable) steps: partial inhibition of N-glycosylation by the SRT pseudosubstrate site followed by recruitment of CCDC134, through interactions with both STT3A and the RLS motif of the pre-N segment, to fully suppress N-glycosylation.

Cotranslational recruitment of CCDC134 to the ER translocon by STT3A and the HSP90B1 nascent chain

To investigate biochemical interactions between CCDC134, HSP90B1, and OST-A, we used a cell-free translation and translocation system that combines rabbit reticulocyte lysate (RRL) with microsomes isolated from human embryonic kidney (HEK) 293T cells of any desired genotype (*35*). Reactions containing wild-type, *CCDC134*$^{-/-}$, *STT3A*$^{-/-}$ or *STT3B*$^{-/-}$ microsomes were programmed with mRNA encoding the 1-93M model substrate derived from HSP90B1 (Fig. 3F). As observed in cells, N-glycosylation of 1-93M was enhanced when it was translated in the presence of microsomes lacking either CCDC134 or STT3A (Fig. 3G) or when it contained the T44A mutation in the pseudosubstrate site (Fig. 3H). N-glycosylation occurs cotranslationally in *CCDC134*$^{-/-}$ microsomes (fig. S8, A and B), as it does in *CCDC134*$^{-/-}$ cells (fig. S7, B and C).

To assess protein interactions during translation and translocation, we used a FLAG-tagged 1-93M construct lacking a stop codon to stall translation, trapping the nascent chain in the ER translocon (Fig. 3F). The stalled

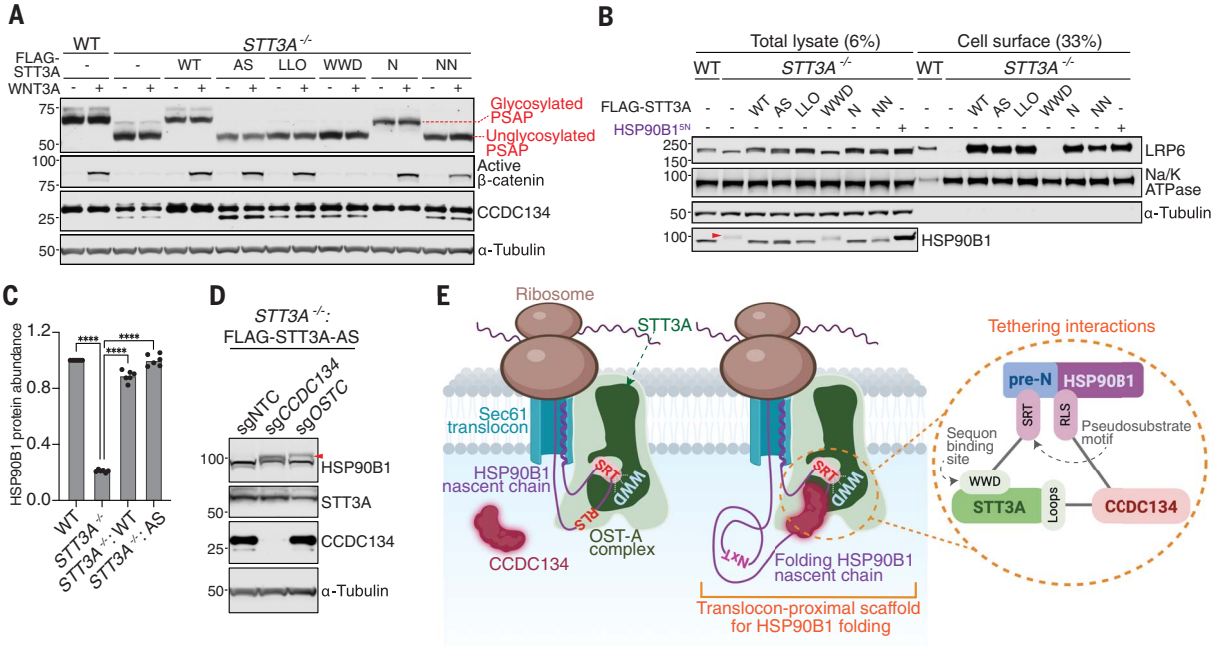

Fig. 4. The oligosaccharyltransferase activity of OST-A is not required to promote HSP90B1 stability and WNT signaling. (**A** and **B**) Glycosylation status and abundances of PSAP (A), active β-catenin (A), CCDC134 (A), HSP90B1 (B), and cell-surface LRP6 (B) in wild-type cells or *STT3A*$^{-/-}$ cells stably expressing FLAG-STT3A variants carrying mutations in various sites involved in catalytic transfer of the glycan from the lipid-linked oligosaccharide to the asparagine in sequons. Variants (shown on a structure in fig. S9A) carry mutations in residues involved in active site chemistry (AS), lipid-linked oligosaccharide binding (LLO), sequon binding (WWD), or N-glycosylation of STT3A itself (N and NN). Glycosylation of PSAP was used to assess OST-A activity in cells. See additional analysis in fig. S9B. (**C**) HSP90B1 protein abundance in wild-type cells, *STT3A*$^{-/-}$ cells, and *STT3A*$^{-/-}$ cells stably expressing wild-type or catalytically inactive (AS) STT3A. The STT3A-AS variant carries mutations in four residues involved in the chemical step of glycan transfer (fig. S9A). Bars represent the mean (N = 6). Statistical significance was determined by one-way ANOVA with Dunnett's test; ****P < 0.0001. (**D**) Abundance and glycosylation status (red arrowhead) of endogenous HSP90B1 in *STT3A*$^{-/-}$ cells stably expressing (i) catalytically inactive FLAG–STT3A-AS carrying mutations in active site residues (fig. S9A) and (ii) sgRNAs targeting CCDC134 or OSTC. sgNTC, nontargeting control sgRNA. (**E**) During translation, HSP90B1 is tethered to a specialized CCDC134-containing translocon that forms a microenvironment for its folding. Tethering interactions suggested by our mutagenesis data are shown in the circular inset: CCDC134 interacts both with STT3A and HSP90B1 (fig. S7, D to H), whereas the pre-N segment of HSP90B1 itself binds to the sequon binding site of STT3A (Figs. 3C and 4A). This translocon-proximal scaffold prevents STT3A from recognizing sequons in HSP90B1 and sterically prevents access of these sequons to OST-B during folding. See fig. S10.

nascent chain was isolated with the FLAG tag, and associated proteins were detected with immunoblotting. As expected for a secretory ER translocon, STT3A, SEC61, and the ribosome were all pulled down with the stalled 1-93M nascent chain (Fig. 3H) (*36*, *37*). CCDC134 was also recruited to this translocon, and its recruitment was dependent on (i) the presence of the 1-93 pre-N segment, (ii) the integrity of the SRT pseudosubstrate site, and (iii) the presence of STT3A (Fig. 3H and fig. S8, C and D). By using stall substrates of various lengths (fig. S8C), we found that CCDC134 was only recruited when the nascent chain was long enough, so that the pre-N sequence of HSP90B1 would be exposed to the lumen of the ER (fig. S8E). Resolving the stall by using puromycin to release the nascent chain from its tRNA conjugate abolished the recruitment of CCDC134, showing that recruitment requires an intact translocon and hence occurs cotranslationally (fig. S8F). Thus, the recruitment of CCDC134 to the secretory translocon assembled by 1-93M in an in vitro reconstituted system is specific and has the same requirements (the pre-N segment, pseudosubstrate site, and STT3A) as those needed to suppress HSP90B1 hyperglycosylation and promote cell-surface LRP6 trafficking and WNT signaling in intact cells.

CCDC134 stabilizes a translocon-proximal protective scaffold for HSP90B1

The observation that OST-A (whose main function is to N-glycosylate proteins) suppresses the N-glycosylation of a specific substrate (HSP90B1) was unexpected. It suggests that OST-A may not function as an enzyme in this context but as a scaffold.

To test this possibility, we used *STT3A*$^{-/-}$ cells to stably express STT3A variants carrying mutations in key residues known to be involved in binding to the lipid-linked oligosaccharide (LLO) (*38*, *39*), binding to the N-X-S/T sequon (*40*), catalyzing the chemical step in LLO transfer to the carboxamide side chain of asparagine (active site residues) (*41*) and in N-glycosylation of STT3A itself (*42*) (fig. S9A). Unlike the complete loss of STT3A, these mutations do not compromise OST-A complex assembly or recruitment to the translocon. As expected, each set of mutations abolished the ability of STT3A to N-glycosylate PSAP (Fig. 4A). Notably, inactive STT3A variants carrying mutations in the active site or LLO binding site were both able to suppress HSP90B1 hyperglycosylation (Fig. 4B and fig. S9B), restore HSP90B1 abundance (Fig. 4C), restore cell-surface levels of LRP6 (Fig. 4B and fig. S9B), and rescue WNT signaling (Fig. 4A). These inactive variants still depended on CCDC134 and the translocon adaptor subunit OSTC to inhibit HSP90B1 hyperglycosylation (Fig. 4D). By contrast, the STT3A variant carrying mutations in the sequon binding site (STT3A-WWD) (fig. S9A) was defective in suppressing HSP90B1 hyperglycosylation and restoring cell surface LRP6 (Fig. 4, A and B, and fig. S9B). Thus, the capacity of STT3A to transfer glycans to proteins is not required for its ability to regulate HSP90B1 hyperglycosylation; however,

its abilities to bind the SRT pseudosubstrate site and associate with the translocon are required.

We propose that the pre-N segment tethers HSP90B1 during its translation, translocation, and folding to translocon-associated OST-A through an interaction between the SRT pseudosubstrate site and the STT3A sequon binding site (Fig. 4E). Two consequences ensue: (i) OST-A is prevented from N-glycosylating subsequent sequons in HSP90B1 as they enter the ER lumen, and (ii) HSP90B1 is sequestered from OST-B until it completes folding, rendering its facultative sequons inaccessible (Fig. 4E and fig. S10). Although the sequon binding site is conserved in STT3B, this model critically depends on the N- to C-terminal scanning mechanism of cotranslational glycosylation, a feature specific to OST-A. CCDC134 functions as a substrate-specific inhibitor, engaging both the substrate (pre-N segment) and enzyme (STT3A) to prevent the N-glycosylation of HSP90B1 (Fig. 4E, inset, and fig. S10). Evolutionary sequence analysis supports a shared function of these proteins. Although HSP90B1 belongs to a clade that dates to the base of the eukaryotic tree (fig. S11A), CCDC134 is a much later invention, found in animals and their sister groups (fig. S11B). It is only within the CCDC134-containing group of organisms that we observe significant constraints on the sequence of the HSP90B1 pre-N segment, including the pseudosubstrate site and surrounding sequence (fig. S11B). Notably, fungi show a concomitant loss of both CCDC134 and sequence conservation in the pre-N segment (fig. S11B). Future structural and reconstitution studies will be necessary to test various predictions of our model and provide definitive insights into the underlying protein interactions and the mechanism of STT3A inhibition.

Discussion

Our work supports the view that custom translocons, tailored by information provided by the nascent chain, can serve as dynamic regulatory platforms to control the biogenesis and fate of secreted and membrane proteins (*36*, *37*, *43*). In this work, we found that the nascent chain recruits CCDC134 to an OST-A–containing translocon to regulate the N-glycosylation and stability of the ER chaperone HSP90B1 with consequences for WNT signaling sensitivity and tissue development. Perhaps the association of OST-A with the translocon, through the dedicated subunits OSTC and KRTCAP2, enabled an expansion of its functions beyond glycan transfer to include serving as a protective microenvironment for folding and quality control that can recruit ER factors to proteins being cotranslationally transported across the ER membrane (*37*). We speculate that ER translocon composition and function may be regulated by signals from the ER or the cytoplasm to regulate cell-cell communication in multicellular organisms.

It remains unclear why such a system has evolved in animals to regulate HSP90B1 activity and, consequently, the reception of diverse developmental, inflammatory, and growth-promoting signals at the cell surface. Key biological questions for the future include how CCDC134 itself is regulated and which cells and tissues during development depend on HSP90B1 hyperglycosylation. Perhaps CCDC134 and HSP90B1 serve to signal the biosynthetic capacity (or some other function) of the ER to the reception of cell surface signals that regulate proliferation or differentiation. Based on its link to the human disease OI, this regulatory mechanism may be particularly important in professional secretory cells, such as osteoblasts, in which (WNT-dependent) differentiation must be coordinated with a massive expansion of the capacity of the ER to synthesize and N-glycosylate secreted components of the bone matrix.

REFERENCES AND NOTES

1. C. Reily, T. J. Stewart, M. B. Renfrow, J. Novak, *Nat. Rev. Nephrol.* **15**, 346–366 (2019).
2. P. Gagneux, T. Hennet, A. Varki, in *Essentials of Glycobiology*, A. Varki *et al*., Eds. (Cold Spring Harbor Laboratory Press, 2022).
3. C. Ruiz-Canada, D. J. Kelleher, R. Gilmore, *Cell* **136**, 272–283 (2009).
4. S. Shrimal, N. A. Cherepanova, R. Gilmore, *J. Cell Biol.* **216**, 3625–3638 (2017).
5. A. S. Ramírez, J. Kowal, K. P. Locher, *Science* **366**, 1372–1375 (2019).
6. K. Braunger *et al*., *Science* **360**, 215–219 (2018).
7. R. Wild *et al*., *Science* **359**, 545–550 (2018).
8. L. Bai, T. Wang, G. Zhao, A. Kovach, H. Li, *Nature* **555**, 328–333 (2018).
9. A. M. Lebensohn *et al*., *eLife* **5**, e21459 (2016).
10. B. Liu *et al*., *Proc. Natl. Acad. Sci. U.S.A.* **110**, 6877–6882 (2013).
11. J.-C. Hsieh *et al*., *Cell* **112**, 355–367 (2003).
12. B. Yu *et al*., *Int. J. Mol. Med.* **41**, 381–390 (2018).
13. DepMap: The Cancer Dependency Map Project at Broad Institute; https://depmap.org/portal/.
14. D. R. Amici *et al*., *Life Sci. Alliance* **4**, 4 (2020).
15. J. Huang *et al*., *Cell. Mol. Life Sci.* **65**, 338–349 (2008).
16. J. Huang *et al*., *Histochem. Cell Biol.* **138**, 41–55 (2012).
17. N. A. Cherepanova, S. V. Venev, J. D. Leszyk, S. A. Shaffer, R. Gilmore, *J. Cell Biol.* **218**, 2782–2796 (2019).
18. D. Dersh, S. M. Jones, D. Eletto, J. C. Christianson, Y. Argon, *Mol. Biol. Cell* **25**, 2220–2234 (2014).
19. R. A. Mazzarella, M. Green, *J. Biol. Chem.* **262**, 8875–8883 (1987).
20. D. Qu, R. A. Mazzarella, M. Green, *DNA Cell Biol.* **13**, 117–124 (1994).
21. S. E. Cala, *Biochim. Biophys. Acta* **1496**, 296–310 (2000).
22. M. L. Medus *et al*., *Sci. Rep.* **7**, 8788 (2017).
23. N. M. Riley, A. S. Hebert, M. S. Westphall, J. J. Coon, *Nat. Commun.* **10**, 1311 (2019).
24. H. H. Freeze, C. Kranz, *Curr. Protoc. Protein Sci.* **12**, 4 (2010).
25. J. Dubail *et al*., *J. Bone Miner. Res.* **35**, 1470–1480 (2020).
26. M. F. Holick, A. Shirvani, N. Charoenngam, *Children (Basel)* **8**, 8 (2021).
27. T. M. Ali *et al*., *Am. J. Med. Genet. A.* **188**, 1545–1549 (2022).
28. M. Jovanovic, G. Guterman-Ram, J. C. Marini, *Endocr. Rev.* **43**, 61–90 (2022).
29. E. A. Ansa-Addo *et al*., *Curr. Top. Med. Chem.* **16**, 2765–2778 (2016).
30. M. Marzec, D. Eletto, Y. Argon, *Biochim. Biophys. Acta* **1823**, 774–787 (2012).
31. D.-S. Kim *et al*., *Cell Death Dis.* **15**, 374 (2024).
32. B. L. Lampson *et al*., *Cell* **187**, 2209–2223.e16 (2024).
33. E. Klaver *et al*., *Dis. Model. Mech.* **12**, 12 (2019).
34. N. A. Cherepanova, R. Gilmore, *Sci. Rep.* **6**, 20946 (2016).
35. A. Sharma, M. Mariappan, S. Appathurai, R. S. Hegde, in *Protein Secretion: Methods and Protocols*, A. Economou, Ed. (Humana Press, 2010), pp. 339–363.
36. A. Sundaram *et al*., *Nature* **611**, 167–172 (2022).
37. M. Gemmer *et al*., *Nature* **614**, 160–167 (2023).
38. M. Napiórkowska *et al*., *Nat. Struct. Mol. Biol.* **24**, 1100–1106 (2017).
39. S. Gerber *et al*., *J. Biol. Chem.* **288**, 8849–8861 (2013).
40. Q. Yan, W. J. Lennarz, *J. Biol. Chem.* **277**, 47692–47700 (2002).
41. C. Lizak, S. Gerber, S. Numao, M. Aebi, K. P. Locher, *Nature* **474**, 350–355 (2011).
42. G. Li, Q. Yan, A. Nita-Lazar, R. S. Haltiwanger, W. J. Lennarz, *J. Biol. Chem.* **280**, 1864–1871 (2005).
43. L. Smalinskaitė, M. K. Kim, A. J. O. Lewis, R. J. Keenan, R. S. Hegde, *Nature* **611**, 161–166 (2022).

ACKNOWLEDGMENTS

We thank R. Kopito, T. Pleiner, R. Gilmore, and J. Carette for generously sharing reagents, insightful discussion, and comments on the manuscript. **Funding:** National Institutes of Health grants GM118082, HD101980, and HD113790 (R.R.); American Cancer Society – Jean Perkins Foundation Postdoctoral Fellowship in Cancer Research, PF-20-121-01-TBE (M.M.); A.P. Giannini Foundation Postdoctoral Fellowship (M.M.); National Institutes of Health intramural funds LM594244 (L.A.); Medical Research Council, as part of United Kingdom Research and Innovation MC_UP_1201/32 (J.F.); National Institutes of Health grant P41 GM108538 and R35 GM118110 (J.J.C.); French association of osteogenesis imperfecta (AOI) (V.C.-D.); Fondation Philanthropia (V.C.-D.). **Author contributions:** Conceptualization: M.M. and R.R.; Methodology: M.M., R.D., A.J., G.V.P., B.S., E.S., K.A.O., V.C.-D., J.F., L.A., and R.R.; Investigation: M.M., R.D., A.J., G.V.P., K.A.O., L.A., and R.R.; Visualization: M.M. and G.V.P.; Funding acquisition: R.R.; Supervision: R.R. and J.J.C.; Writing – original draft: M.M. and R.R.; Writing – review and editing: M.M., G.V.P., R.D., A.J., J.F., L.A., and R.R. **Competing interests:** JJC is a consultant for Thermo Fisher Scientific, Seer, and 908 Devices. The Other authors declare that they have no competing interests. **Data and materials availability:** All unique reagents generated in this study are available from the corresponding author and will be provided upon request. All data are available in the manuscript or the supplementary materials. This paper does not report original code. All FASTQ files from CRISPR-Cas9 screen have been deposited into the NIH Short Read Archive (SRA) with BioProject accession number PRJNA1087438. Raw data files for N-glycoproteomic analyses have been deposited into the MassIVE database under the accession number MSV000094280. All patient fibroblast cells used in this manuscript have been previously established by V.C.-D. and reported in a prior peer-reviewed publication from their laboratory (*25*). Informed consent for participation and sample collection were obtained through protocols approved by the Necker-Enfants Malades Hospital, AP-HP, F-75015 Paris, France. This work used only these previously published unidentifiable or deidentified cell lines and did not involve any active patient recruitment or new sample collection from patients.

SUPPLEMENTARY MATERIALS

science.org/doi/10.1126/science.adp7201
Materials and Methods
Figs. S1 to S11
References (*44*–*60*)
Data S1 and S2

Submitted 10 April 2024; resubmitted 25 July 2024
Accepted 19 September 2024
10.1126/science.adp7201